WASP-128b

Hodžić, V.; Triaud, A. H. M. J.; Anderson, D. R.; Bouchy, F.; Cameron, A. Collier; Delrez, L.; Gillon, M.; Hellier, C.; Jehin, E.; Lendl, M.; Maxted, P. F. L.; Pepe, F.; Pollacco, D.; Queloz, D.; Ségransan, D.; Smalley, B.; Udry, S.; West, R.

DOI:
10.1093/mnras/sty2512

Monthly Notices
of the
ROYAL ASTRONOMICAL SOCIETY

MNRAS **481,** 5091–5097 (2018)
Advance Access publication 2018 September 14

doi:10.1093/mnras/sty2512

WASP-128b: a transiting brown dwarf in the dynamical-tide regime

Vedad Hodžić,[1]★ Amaury H. M. J. Triaud,[1] David R. Anderson,[2] François Bouchy,[3] Andrew Collier Cameron,[4] Laetitia Delrez,[5] Michaël Gillon,[6] Coel Hellier,[2] Emmanuël Jehin,[6] Monika Lendl,[7,3] Pierre F. L. Maxted,[2] Francesco Pepe,[3] Don Pollacco,[8] Didier Queloz,[5,3] Damien Ségransan,[3] Barry Smalley,[2] Stéphane Udry,[3] and Richard West[8]

[1]*School of Physics and Astronomy, University of Birmingham, Edgbaston, Birmingham B15 2TT, UK*
[2]*Astrophysics Group, Keele University, Staffordshire ST5 5BG, UK*
[3]*Observatoire de Genève, Université de Genève, Chemin des Maillettes 51, CH-1290 Sauverny, Switzerland*
[4]*Centre for Exoplanet Science, SUPA School of Physics and Astronomy, University of St. Andrews, North Haugh, Fife KY16 9SS, UK*
[5]*Cavendish Laboratory, J J Thomson Avenue, Cambridge CB3 0HE, UK*
[6]*Institut d'Astrophysique et de Géophysique, Université de Liège, Allée du 6 Août, 17, Bat. B5C, Liège 1, Belgium*
[7]*Space Research Institute, Austrian Academy of Sciences, Schmiedlstr. 6, A-8042 Graz, Austria*
[8]*Department of Physics, University of Warwick, Gibbet Hill Road, Coventry CV4 7AL, UK*

Accepted 2018 August 28. Received 2018 August 27; in original form 2018 July 26

ABSTRACT

Massive companions in close orbits around G dwarfs are thought to undergo rapid orbital decay due to runaway tidal dissipation. We report here the discovery of WASP-128b, a brown dwarf discovered by the WASP survey transiting a G0V host on a 2.2 d orbit, where the measured stellar rotation rate places the companion in a regime where tidal interaction is dominated by dynamical tides. Under the assumption of dynamical equilibrium, we derive a value of the stellar tidal quality factor $\log Q'_\star = 6.96 \pm 0.19$. A combined analysis of ground-based photometry and high-resolution spectroscopy reveals a mass and radius of the host, $M_\star = 1.16 \pm 0.04\,\mathrm{M}_\odot$, $R_\star = 1.16 \pm 0.02\,\mathrm{R}_\odot$, and for the companion, $M_\mathrm{b} = 37.5 \pm 0.8\,M_\mathrm{J}$, $R_\mathrm{b} = 0.94 \pm 0.02\,R_\mathrm{J}$, placing WASP-128b in the driest parts of the brown dwarf desert, and suggesting a mild inflation for its age. We estimate a remaining lifetime for WASP-128b similar to that of some ultra-short period massive hot Jupiters, and note it may be a propitious candidate for measuring orbital decay and testing tidal theories.

Key words: methods: data analysis – planets and satellites: dynamical evolution and stability – binaries: eclipsing – brown dwarfs.

1 INTRODUCTION

Brown dwarfs are substellar objects that occupy the mass range ∼13–80 Jupiter masses, (M_J), thought to form via gravitational instability or molecular cloud fragmentation (Chabrier et al. 2014). Despite their abundance, however, very little is known about brown dwarfs. Most are found to be solitary, show complex spectral features that are difficult to model, and their masses are typically hard to estimate because the models are degenerate with their age, radius, and metallicity. Brown dwarf companions orbiting Sun-like stars offer a chance to study these objects in more detail as the stellar ages can be tied to the orbiting brown dwarf. Moreover, transit light curves can lift the inclination angle degeneracy to yield an unambiguous mass from radial velocity measurements, providing precise physical parameters that are crucial for testing substellar evolutionary models.

Despite being fully sensitive throughout the brown dwarf mass range, early Doppler surveys reported that brown dwarf companions are found in fewer numbers than their free-floating counterparts, termed the *brown dwarf desert* (Marcy & Butler 2000; Sahlmann et al. 2011; Ma & Ge 2014). When comparing the same sample of host stars, up to 16 per cent of Sun-like stars have companions more massive than Jupiter, of which <1 per cent are brown dwarfs (Grether & Lineweaver 2006). Only 12 transiting brown dwarfs have been found to date (Bayliss et al. 2017 and references therein, Cañas et al. 2018), where just three have been detected from the ground, possibly due to a detection bias (Csizmadia et al. 2015). Only one other brown dwarf has been discovered by

★ E-mail: vxh710@bham.ac.uk

the WASP survey (WASP-30b; Anderson et al. 2011; Triaud et al. 2013).

Most massive substellar companions on close orbits have been found around F-type stars, and very few around G dwarfs, which has been interpreted as being due to rapid engulfment of massive planets and brown dwarfs around G dwarfs due to strong tidal coupling (Bouchy et al. 2011; Guillot et al. 2014; Damiani & Díaz 2016). Stars generally spin down as they age due to magnetic braking, where stellar winds carry highly ionized material that couples to the magnetic field lines and gets carried away from the star, leading to angular momentum loss. G dwarfs are typically more efficient at magnetic braking due to their deeper outer convective layer. However, companions on close orbits can transfer angular momentum from the orbit to the stellar spin, thereby draining angular momentum from the system via magnetic braking, leading to orbital decay until the companion is engulfed by the host. The rate of the companion's orbital decay is predicted to increase by up to three orders of magnitude in the dynamical-tide regime (Ogilvie & Lin 2007), with observational evidence on hot Jupiter hosts supporting stronger tidal coupling than for equilibrium tides (Collier Cameron & Jardine 2018). The strong dynamical tides from the companion excite inertial gravity waves (g-modes) in the convective layer that, in G dwarfs, break and dissipate in the radiative core, resulting in a spin-up the star from the inside (Barker & Ogilvie 2010; Essick & Weinberg 2016). Thus, in systems where the host stars can be spun up by a massive companion such as a brown dwarf, the strong tidal coupling is expected to lead to runaway orbital decay of the companion on to the central star on short time-scales compared to the lifetime of the star (Barker & Ogilvie 2010).

In this context, we report the discovery of WASP-128b, a new transiting brown dwarf discovered by the WASP survey, orbiting a G0V host on a close orbit, where the measured stellar rotation rate places the system well-within the dynamical-tide regime, suggesting strong tidal coupling between the pair.

2 OBSERVATIONS

2.1 Photometry

WASP-128 is a moderately bright ($V = 12.5$) G0V star at a distance of 422 ± 5 pc. The WASP survey (Pollacco et al. 2006) obtained 31 543 images of WASP-128 between 2006 May 04 and 2012 Dec. 19, identifying a periodic 2.208 d transit signal in the photometry (Collier Cameron et al. 2006). Consequently, we initiated photometric and spectroscopic follow-up observations.

Five transits of WASP-128b were obtained using the 0.6 m TRAPPIST robotic telescope (Gillon et al. 2011; Jehin et al. 2011), located at ESO La Silla Observatory (Chile). The first of these transit observations is partial, covering only the second half of the transit. All five transits were observed through a 'blue-blocking' filter. The images are calibrated using standard procedures (bias, dark, and flat-field correction) and photometry is extracted using the IRAF/DAOPHOT[1] aperture photometry software (Stetson 1987), as described by Gillon et al. (2013). For each transit observation, a careful selection of both the photometric aperture size and stable comparison stars is performed manually to obtain the most accurate differential light curve of WASP-128. Some light curves are affected by a meridian flip; that is, the 180° rotation that TRAPPIST's equatorial mount has to undergo when the meridian is reached. We account for any potential photometric offset in our baseline model, see Section 3.2.

We observed three transits of WASP-128b using the EulerCam instrument installed at the 1.2 m *Euler* telescope also located at the La Silla site. The observations were carried out through an r'-Gunn filter and the telescope was slightly defocused to improve PSF sampling and observation efficiency. Each transit light curve is obtained using relative aperture photometry while optimizing reference star selection and extraction apertures to minimize the residual light curve rms. The instrument and the associated data reduction is described in more detail in Lendl et al. (2012). Some of the images of WASP-128 leading up to and during the ingress of the second transit were saturated, and as such, we discarded a handful of observations in our analysis that had count levels above 50 000 ADU.

2.2 Spectroscopy

We collected 48 spectra from the CORALIE spectrograph on the *Euler* telescope between 2013-06-06 and 2016-11-24, as well as 23 HARPS spectra on the ESO 3.6 m telescope between 2015 April 02 and 2018 March 22. Both sets of data are reduced using similar data reduction softwares. Their resulting spectra are correlated with a numerical mask matching a G2V star (Baranne et al. 1996; Pepe et al. 2002). These procedures have been demonstrated to reach high precision and high accuracy (e.g. Mayor et al. 2009; López-Morales et al. 2014). We perform a single 3σ-clip on each radial velocity set using the line full width at half-maximum (FWHM) and bisector inverse slope span (BIS). One HARPS observation is discarded due to a highly discrepant BIS value, and one CORALIE observation was discarded due to the FWHM clip. Those outliers are highlighted in Appendix A.

3 DATA ANALYSIS

3.1 Spectral analysis

Using methods similar to those described by Doyle et al. (2013), we used the co-added HARPS spectrum to determine values for stellar effective temperature $T_{\rm eff}$, surface gravity $\log g_\star$, metallicity [Fe/H], and projected stellar rotational velocity $v \sin i_\star$. In determining $v \sin i$ we assumed a macroturbulent velocity of 4.4 ± 0.7 km s^{-1}, based on the asteroseismic calibration of Doyle et al. (2014). Using MKCLASS (Gray & Corbally 2014), we obtain a spectral-type G0V for WASP-128, which is consistent with the temperature derived from the spectral analysis. The Lithium abundance $\log A(\mathrm{Li}) = 2.62 \pm 0.09$ suggests a relatively young age of 1–2 Gyr.

3.2 Global modelling

The combined data are analysed using AMELIE, a novel software package that jointly models the photometric and radial velocity data in a standard Bayesian framework. The code is essentially a PYTHON wrapper on the `ellc` binary star light-curve model (Maxted 2016) for computing exoplanet and eclipsing binary light curves and their radial velocity orbits, and the EMCEE affine-invariant Markov chain Monte Carlo (MCMC) sampler (Goodman & Weare 2010;

[1] IRAF is distributed by the National Optical Astronomy Observatory, which is operated by the Association of Universities for Research in Astronomy, Inc., under cooperative agreement with the National Science Foundation.

Foreman-Mackey et al. 2013) for exploring the posterior parameter space.

We adopt a quadratic limb darkening law to model the intensity distribution of the stellar disc, using the LDTKpackage (Husser et al. 2013; Parviainen & Aigrain 2015) to sample band-specific limb darkening coefficients for the *Euler* and TRAPPIST data sets, following the triangular parametrization described in Kipping (2013). No priors are imposed on the limb darkening parameters, rather, we fit the intensity profile of the disc using the built-in likelihood function, allowing uncertainties in the spectral parameters to be propagated to our final result. In addition, we sample the following parameters for our transit and radial velocity model: Period, P; mid-transit reference time, T_0; transit depth, D; transit width (time from first to fourth contact), W; impact parameter, b; and radial velocity semi-amplitude, K. Moreover, for our eccentric model we also sample the parameters $\sqrt{e}\sin\omega$ and $\sqrt{e}\cos\omega$, and in our orbital decay model we further sample $\dot{P} = \mathrm{d}P/\mathrm{d}t$. In all cases we use non-informative priors that are either physically bounded (e.g. $0 < b < 1$) or sensibly bounded to a wide enough region (e.g. $0 < K < 50\,\mathrm{km\,s^{-1}}$), where the transit mid-point is bounded by the light curves on 2014 March 03.

For each sampled set of parameters we further compute photometric and radial velocity baseline models. Our photometric baseline model consists of a normalization factor with a second-order polynomial in time for each light curve to allow for airmass and seeing effects. Moreover, we experimented with additional photometric detrending using sky background levels, FWHM changes in the PSF, and changes in the target pixel position on the CCD. Using the Bayesian Information Criterion (BIC; Schwarz 1978) to compare model complexity, we find that an additional first-order polynomial using sky background levels is strongly preferred for the *Euler* light curve on 2014 March 25. On the nights of 2014 Feb. 11, 2014 March 03, and 2015 May 10, the TRAPPIST telescope peformed a meridian flip, for which we account for any potential offsets by allowing an additional normalization factor before the flip. The radial velocity baseline model consists of a constant systemic velocity for each instrument. The CORALIE data are partitioned into two data sets due to an upgrade of the instrument that could affect the velocity zero-point (Triaud et al. 2017). We compare the constant velocity model with models allowing a first- and second-order drift term, but find that any higher order terms are unjustified. The baseline model parameters are computed using a least-squares algorithm for every proposed parameter set in the MCMC sampling. Finally, we also sample additional errors on our photometry and radial velocity data to account for underestimated errors due to instrumental effects and stellar activity.

The mean stellar density can be estimated independently from a transit light curve and can be used with other observables to constrain the mass and age of a star from stellar evolution models (Seager & Mallén-Ornelas 2003; Triaud et al. 2013). We use BAGEMASS (Maxted, Serenelli & Southworth 2015) to estimate the age and mass of the host star, using our estimates of $T_{\rm eff}$ and [Fe/H] from the spectral modelling in Section 3.1, luminosity from *Gaia* DR2 (Andrae et al. 2018), and the mean stellar density from the transit light curves as inputs to the code. The mass is then used as input to our Keplerian model.

We initiate 256 walkers at positions normally dispersed close to the solution, and run each walker for 30 000 steps, chosen such that each walker is run for a few tens of autocorrelation lengths after discarding the first 15 000 steps as burn-in. The independent chains were thinned by a factor 100 due to autocorrelation, leaving each parameter with 38 400 independent samples, before computing the $\hat{R}$ statistic (Gelman et al. 2003), and mixing the chains. All parameters reach the recommended $\hat{R} < 1.1$, indicating overall convergence.

4 RESULTS

Using BAGEMASS we find an age of 2.3 ± 0.9 Gyr and mass of $M_\star = 1.16 \pm 0.04\,\mathrm{M_\odot}$ for WASP-128. From this we derive a radius of the star of $R_\star = 1.16 \pm 0.02\,\mathrm{R_\odot}$, and mass and radius of $M_\mathrm{b} = 37.5 \pm 0.8\,M_\mathrm{J}$ and $R_\mathrm{b} = 0.94 \pm 0.02\,R_\mathrm{J}$, for the companion, placing it securely in the brown dwarf regime. The best-fitting models with the photometric data are shown in Fig. 1, and in Fig. 2 for the radial velocity data. The results from our MCMC and derived parameters are shown in Table 1 with their 68 per cent confidence interval.

Eccentric model. Given the close proximity to the host star, it is expected that the orbit of WASP-128b has been tidally circularized due to tidal dissipation in the brown dwarf as this would happen on a time-scale of $\leq$1 Gyr (Barker & Ogilvie 2009). Nevertheless, when including eccentricity in our model, we derive a value of $e = 0.003^{+0.003}_{-0.002}$. Observational errors can lead to the detection of a small, non-zero, but spurious eccentricity (Lucy & Sweeney 1971). The BIC strongly disfavours an eccentric model compared to a circular fit. We apply the revised Lucy-Sweeney test (Lucy 2013) to put an upper limit of $e < 0.007$ on the eccentricity using their uniform prior. The results of the other parameters between the two models are consistent with each other, and as such we present the results from the circular fit in Table 1, with our upper limit on the eccentricity.

Orbital decay model. A periodic signal of 2.93 ± 0.03 d was found in the photometric data (Maxted et al. 2011), which is consistent with the derived rotation period of $P_\star = 2.93 \pm 0.18$ d for WASP-128, using the observed $v \sin i_\star$ and $R_\star$. The fast rotation for an early G dwarf could indicate a tidal spin-up due to its massive companion. Given the expected strong tidal coupling in this system, we attempted to directly measure an orbital decay in the radial velocity data by including a period time-derivative, $\dot{P}$ in our model. We find that $\dot{P} = 1.05^{+1.13}_{-1.14}\,\mathrm{s\,yr^{-1}}$, and note that, although not significant, we would not expect a positive $\dot{P}$ in our case where $P_\mathrm{orb} < P_\star$.

5 DISCUSSION

5.1 Tidal evolution

The orbital decay of the companion is significantly affected by magnetic braking as long as the total angular momentum of the system can remain above the critical limit (Damiani & Lanza 2015; Damiani & Díaz 2016),

$$L_\mathrm{crit} = 4\left(\frac{G^2}{27}\frac{M_\star^3 M_\mathrm{b}^3}{M_\star + M_\mathrm{b}}(\beta(t) I_\star + I_\mathrm{b})\right)^{\frac{1}{4}},$$

where $I = \alpha M R^2$ is the moment of inertia of the two objects, defined by their effective squared radii of gyration, α. The inclusion of $\beta(t)$ extends the original work by Hut (1980) to include the effects of orbital evolution due to magnetic braking, where $\beta = \Omega/n$ is the ratio of the stellar rotation rate to the orbital frequency, with $n^2 = G(M_\star + M_\mathrm{b})/a^3$. When $L > L_\mathrm{crit}$, the system can enter a pseudo-equilibrium state which is stable if the orbital angular momentum

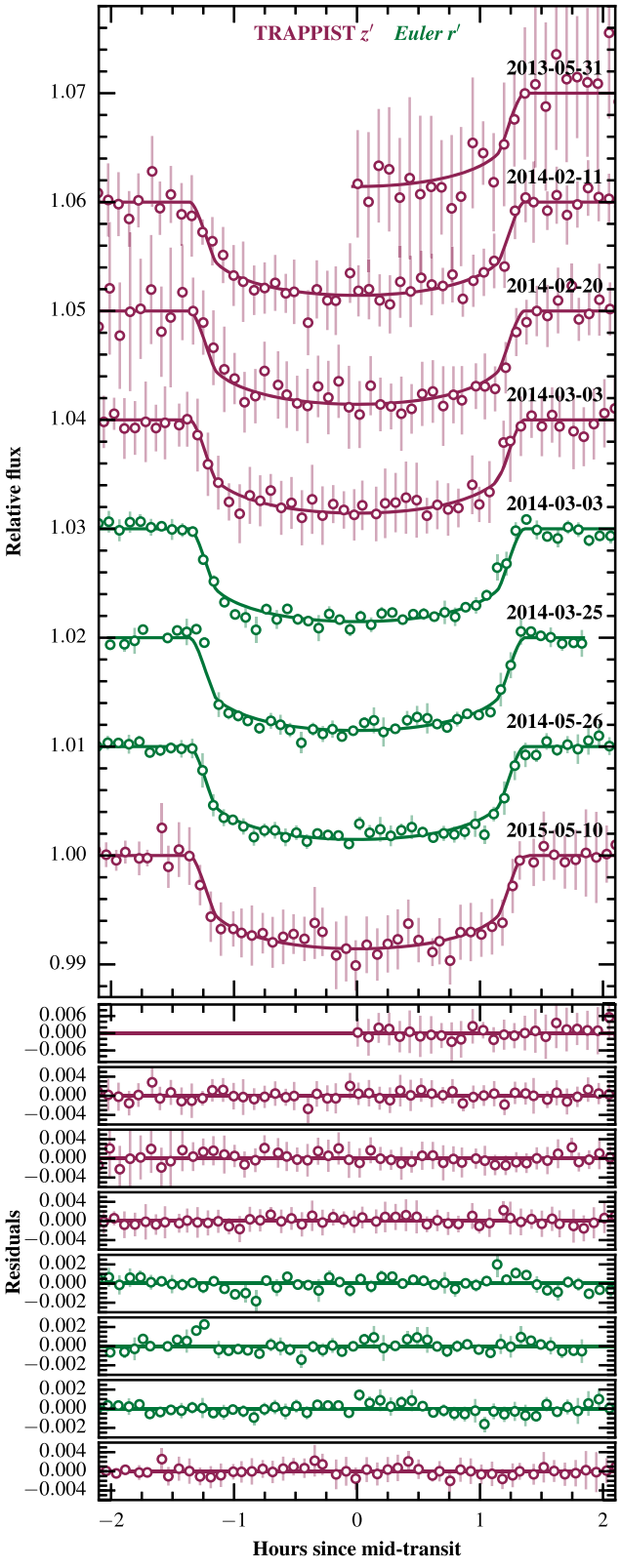

Figure 1. Transits of WASP-128 taken with the *Euler* (*green*) and TRAPPIST (*vermillion*) telescopes. The points correspond to detrended data binned to 5 min, and the coloured lines are the best-fitting models. The residuals of the fit are shown in the lower panel.

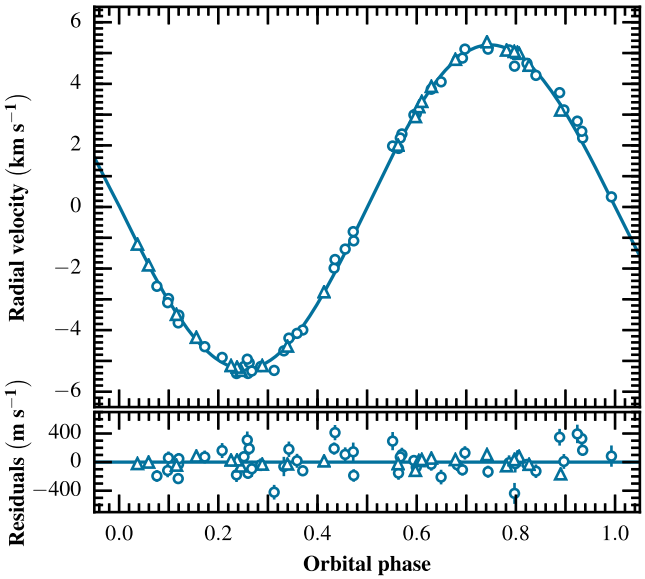

Figure 2. The radial velocity motion of WASP-128 due to its brown dwarf companion, folded on the best-fitting period. The blue points correspond to RV measurements taken with CORALIE (*circles*) and HARPS (*triangles*). The solid line is the best-fitting model. The residuals of the fit are shown in the lower panel.

Table 1. WASP-128 system information and results. Numbers in brackets denote uncertainties on the last two digits from the 16th and 84th percentiles. ⋆ and 'b' subscripts denote the host star and companion, respectively.

WASP-128
$11^{h}31^{m}26\overset{s}{.}10\ -41^{\circ}41'22\overset{''}{.}3$
2MASS J11312609-4141222
Gaia 5382697351745548416

Parameter	Value	Unit	Parameter	Value	Unit
Spectral and system parameters					
$T_{\rm eff}$	5950 ± 50	K	d	422 ± 6	pc
$\log g_\star$	4.1 ± 0.1	cgs	$\tau_\star$	2.2 ± 0.9	Gyr
[Fe/H]	0.01 ± 0.12	dex	$G_{\rm mag}$	12.3	
$v \sin i_\star$	20.0 ± 1.2	km s^{-1}	Sp. type	G0V	
Sampled parameters					
P	$2.208524^{(+21)}_{(-20)}$	d	K	$5.272^{(+16)}_{(-16)}$	km s^{-1}
T_0	$2456720.68369^{(+19)}_{(-19)}$	$\rm BJD_{UTC}$	$q_1(r')$	$0.3679^{(+12)}_{(-12)}$	
D	$0.00699^{(+15)}_{(-15)}$		$q_2(r')$	$0.39437^{(+92)}_{(-92)}$	
W	$0.11290^{(+48)}_{(-44)}$	d	$q_1(z')$	$0.3805^{(+12)}_{(-12)}$	
b	$0.11^{(+10)}_{(-07)}$	$R_\star$	$q_2(z')$	$0.39827^{(+89)}_{(-89)}$	
Derived parameters					
$M_\star$	$1.155^{(+39)}_{(-39)}$	$M_\odot$	$M_{\rm b}$	$37.19^{(+83)}_{(-85)}$	$M_{\rm J}$
$R_\star$	$1.152^{(+21)}_{(-16)}$	$R_\odot$	$R_{\rm b}$	$0.937^{(+22)}_{(-18)}$	$R_{\rm J}$
$R_\star/a$	$0.1489^{(+24)}_{(-09)}$		$R_{\rm b}/a$	$0.01246^{(+27)}_{(-18)}$	
$\rho_\star$	$0.807^{(+16)}_{(-38)}$	$\rho_\odot$	$\rho_{\rm b}$	$55.9^{+2.6}_{-3.5}$	g cm^{-3}
$\log g_\star$	$4.396^{(+08)}_{(-14)}$	cgs	$\log g_{\rm b}$	$5.040^{(+13)}_{(-18)}$	cgs
a	$0.03590^{(+38)}_{(-40)}$	AU	i	$89.10^{(+63)}_{(-91)}$	$^\circ$
$M_{\rm b}/M_\star$	$0.03074^{(+37)}_{(-35)}$		$f(m)$	$0.0000316^{(+03)}_{(-03)}$	$M_\odot$
$R_{\rm b}/R_\star$	$0.08359^{(+89)}_{(-88)}$		e	<0.007	

$L_{\rm orb}$ satisfies

$$L_{\rm orb} > (4 - \beta(t))(I_\star + I_{\rm b})n.$$

The companion satisfies both these criteria, so is thus either evolving towards the dynamically stable state, or is already in synchronization. Under the assumption of the latter, we can derive the stellar tidal dissipation parameter $Q'_\star$ that is needed to balance the tidal torque with the wind braking torque using relations in e.g. Brown et al. (2011) and Damiani & Díaz (2016), finding $\log Q'_\star = 6.96 \pm 0.19$. Recently, Collier Cameron & Jardine (2018) presented a study of the hot Jupiter population that yielded a value of $\log Q'_\star = 8.26 \pm 0.14$. In the regime where $0.5 < P/P_\star < 2$, dynamical tide become important (Ogilvie & Lin 2007). For a subset of hot Jupiters that fall into this range, the tidal dissipation parameter was found to be an order of magnitude smaller, where $\log Q'_\star = 7.31 \pm 0.39$, which is consistent with our estimate. In fact, using the above estimate for $Q'_\star$, we derive that the spin period of the star needed for a dynamically stable state is $2.80^{+0.44}_{-0.26}$ d, which increases confidence in our assumption about spin-orbit synchronization. While in the dynamically stable state, the infall time of WASP-128b is given by the magnetic braking time-scale, and we derive a remaining lifetime of 267^{+145}_{-67} Myr. In reality this is a lower limit, as the infall time will not be driven by magnetic braking once the companion is below the critical orbital period needed to stay in the dynamically stable state. Thereafter, the infall will proceed more slowly, but will still reach the Roche limit within a few tens of Myr (fig. 3, Damiani & Díaz 2016).

More generally, lifetime estimates depend on the structural and rotational evolution of stars (Bolmont & Mathis 2016; Gallet et al. 2017). Using $\log Q'_\star = 6$ and implementing a dynamical model that includes tidal interactions between the star and companion, stellar evolution, magnetic braking, and tidal dissipation by gravity waves, Guillot et al. (2014) predicts a survival time of 50–60 per cent of the host's main-sequence lifetime for a companion at the mass of WASP-128b initially at a 3 d orbit. The main-sequence lifetime of WASP-128 with a mass of about 1.16 $M_\odot$ is ∼6.9 Gyr, which corresponds to a lifetime of 3.5–4.2 Gyr for WASP-128b. The age estimated from BAGEMASS could thus be consistent with the companion's survival, although a thorough calculation of the companion's evolutionary history is needed to estimate its initial location (Brown et al. 2011).

5.2 Inflation

In Fig. 3, we place WASP-128b in a mass–radius diagram with the other known transiting brown dwarfs. WASP-128b sits in the driest part of the brown dwarf desert, $35 < m \sin i < 55$ $M_{\rm J}$ (Sahlmann et al. 2011; Ma & Ge 2014), coinciding with the ∼45 $M_{\rm J}$ mass minimum found in Grether & Lineweaver (2006). It has been suggested that this minimum separates two brown dwarf populations differing by their formation mechanisms: The first formed in the protoplanetary disc via gravitational instability, and the second through molecular cloud fragmentation (Ma & Ge 2014). In this context, WASP-128b clearly belongs to the low-mass population of brown dwarfs.

Using our mass and age estimates for WASP-128b, the COND03 evolutionary models (Baraffe et al. 2003) predict a radius of 0.90 $R_{\rm J}$, which suggests a mild inflation compared to the measured radius. Irradiation effects should have little impact in inflating brown dwarfs, thus it is more likely due to some other mechanism that deposits energy in the brown dwarf interior (Bouchy et al. 2011).

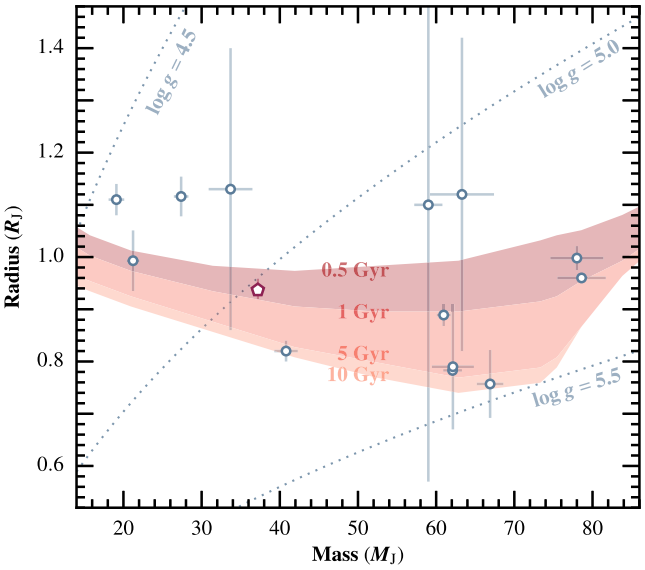

Figure 3. Mass–radius diagram placing WASP-128b (*vermillion*) in the context of the other known transiting brown dwarfs. Objects are from Bayliss et al. (2017) and references therein, including the recent discovery of Kepler-503b (Cañas et al. 2018). The shaded area outlines isochrones for substellar objects from the COND03 models (Baraffe et al. 2003).

6 CONCLUSION

We have discovered WASP-128b, a transiting brown dwarf from the WASP survey on a 2.2 d orbit around a G dwarf. Dynamical-tide theory predicts very few such objects should exist due to rapid orbital decay from strong stellar tidal coupling. Using radial velocity data collected over ∼5 yr, we rule out any significant orbital decay, and we derive a value of the stellar tidal quality factor based on an assumption of dynamical stability. The derived age, mass, and size of WASP-128b suggest a mild inflation, although we cannot rule out a young age.

ACKNOWLEDGEMENTS

The authors are grateful to the anonymous referee for providing useful comments. This study was carried out using data collected at ESO's La Silla Observatory, Chile: HARPS on the ESO 3.6m (Prog IDs 095.C-0105 & 097.C-0434), the Swiss *Euler* telescope, and TRAPPIST. The data are publicly available at CDS, and on demand to the main author. We would like to thank the kind attention of the ESO staff at La Silla, and the many observers who collected data with CORALIE and HARPS along the years. VH is supported by the School of Physics & Astronomy at the University of Birmingham, as well a generous grant through the Postgraduate Research Scholarship Fund at the University of Birmingham. This work has made use of data from the European Space Agency (ESA) mission *Gaia* (https://www.cosmos.esa.int/gaia), processed by the *Gaia* Data Processing and Analysis Consortium (DPAC, https://www.cosmos.esa.int/web/gaia/dpac/consortium). Funding for the DPAC has been provided by national institutions, in particular the institutions participating in the *Gaia* Multilateral Agreement. This research also made use of Astropy, a community-developed core PYTHON package for Astronomy (The Astropy Collaboration 2018), as well as the open-source PYTHON packages NUMPY (Walt, Colbert & Varoquaux 2011), SCIPY (Jones et al. 2001), and MATPLOTLIB (Hunter 2007).

REFERENCES

Anderson D. R. et al., 2011, ApJ, 726, L19
Andrae R. et al., 2018, A&A, 616, A8
Baraffe I., Chabrier G., Barman T. S., Allard F., Hauschildt P. H., 2003, A&A, 402, 701
Baranne A. et al., 1996, A&AS, 119, 373
Barker A. J., Ogilvie G. I., 2009, MNRAS, 395, 2268
Barker A. J., Ogilvie G. I., 2010, MNRAS, 404, 1849
Bayliss D. et al., 2017, AJ, 153, 15
Bolmont E., Mathis S., 2016, Celest. Mech. Dyn. Astron., 126, 275
Bouchy F. et al., 2011, A&A, 525, A68
Brown D. J. A., Collier Cameron A., Hall C., Hebb L., Smalley B., 2011, MNRAS, 415, 605
Cañas C. I. et al., 2018, ApJ, 861, L4
Chabrier G., Johansen A., Janson M., Rafikov R., 2014, Protostars and Planets VI. University of Arizona Press, Tucson, p. 619
Collier Cameron A., Jardine M., 2018, MNRAS, 476, 2542
Collier Cameron A. et al., 2006, MNRAS, 373, 799
Csizmadia S. et al., 2015, A&A, 584, A13
Damiani C., Díaz R. F., 2016, A&A, 589, A55
Damiani C., Lanza A. F., 2015, A&A, 574, A39
Doyle A. P. et al., 2013, MNRAS, 428, 3164
Doyle A. P., Davies G. R., Smalley B., Chaplin W. J., Elsworth Y., 2014, MNRAS, 444, 3592
Essick R., Weinberg N. N., 2016, ApJ, 816, 18
Foreman-Mackey D., Hogg D. W., Lang D., Goodman J., 2013, PASP, 125, 306
Gallet F., Bolmont E., Mathis S., Charbonnel C., Amard L., 2017, A&A, 604, A112
Gelman A., Carlin J., Stern H., Rubin D., 2003, Bayesian Data Analysis, 2nd edn. Chapman & Hall/CRC Texts in Statistical Science, Taylor & Francis
Gillon M., Jehin E., Magain P., Chantry V., Hutsemékers D., Manfroid J., Queloz D., Udry S., 2011, EPJ Web Conf. p. 06002
Gillon M. et al., 2013, A&A, 552, A82
Goodman J., Weare J., 2010, Commun. Appl. Math. Comput. Sci., 5, 65
Gray R. O., Corbally C. J., 2014, AJ, 147, 80
Grether D., Lineweaver C. H., 2006, ApJ, 640, 1051
Guillot T., Lin D. N. C., Morel P., Havel M., Parmentier V., 2014, EAS Publ. Ser. Vol. 65, Evolution of Exoplanets and Their Parent Stars. Cambridge Univ. Press, Cambridge, p. 327
Hunter J. D., 2007, Comput. Sci. Eng., 9, 90
Husser T.-O., Wende-von Berg S., Dreizler S., Homeier D., Reiners A., Barman T., Hauschildt P. H., 2013, A&A, 553, A6
Hut P., 1980, A&A, 92, 167
Jehin E. et al., 2011, Messenger, 145, 2
Jones E. et al., 2001, SciPy: Open Source Scientific Tools for Python. Available at: http://www.scipy.org/
Kipping D. M., 2013, MNRAS, 435, 2152
Lendl M. et al., 2012, A&A, 544, A72
López-Morales M. et al., 2014, ApJ, 792, L31
Lucy L. B., 2013, A&A, 551, A47
Lucy L. B., Sweeney M. A., 1971, AJ, 76, 544
Ma B., Ge J., 2014, MNRAS, 439, 2781
Marcy G. W., Butler R. P., 2000, PASP, 112, 137
Maxted P. F. L., 2016, A&A, 591, A111
Maxted P. F. L. et al., 2011, PASP, 123, 547
Maxted P. F. L., Serenelli A. M., Southworth J., 2015, A&A, 575, A36
Mayor M. et al., 2009, A&A, 493, 639
Ogilvie G. I., Lin D. N. C., 2007, ApJ, 661, 1180
Parviainen H., Aigrain S., 2015, MNRAS, 453, 3821
Pepe F. et al., 2002, Messenger, 110, 9
Pollacco D. L. et al., 2006, PASP, 118, 1407
Sahlmann J. et al., 2011, A&A, 525, A95
Schwarz G., 1978, Ann. Stat., 6, 461
Seager S., Mallén-Ornelas G., 2003, ApJ, 585, 1038
Stetson P. B., 1987, PASP, 99, 191
The Astropy Collaboration, 2018, AJ, 156, A33
Triaud A. H. M. J. et al., 2013, A&A, 549, A18
Triaud A. H. M. J. et al., 2017, MNRAS, 467, 1714
Walt S. v. d., Colbert S. C., Varoquaux G., 2011, Comput. Sci. Eng., 13, 22

APPENDIX A: RADIAL VELOCITIES

Table A1. HARPS radial velocity data set. Machine readable format is available online at CDS.

BJD_{UTC}	RV ($km\,s^{-1}$)	σ ($km\,s^{-1}$)	FWHM ($km\,s^{-1}$)	BIS ($km\,s^{-1}$)
57114.604490	10.19886	0.03857	28.02641	0.65954
57114.767777	11.96217	0.03481	28.04199	0.49807
57115.580569	19.81497	0.03248	28.21436	− 0.43354
57115.821461	17.86571	0.03447	28.53128	− 0.25040
57116.701126	9.56556	0.03357	27.96543	0.04673
57135.560277[a]	19.32195	0.04225	28.00931	− 212.09835
57137.581652	20.08288	0.03328	28.06999	− 0.14360
57138.694412	9.41227	0.03810	27.94346	− 0.07837
57139.649675	19.51470	0.03889	27.97368	− 0.00470
57141.695657	17.97551	0.03256	28.06352	− 0.23932
57157.596595	19.73995	0.03206	27.75519	− 0.30482
57158.556607	9.51614	0.02926	27.90052	− 0.15205
57181.510526	18.63475	0.03266	27.77245	− 0.24299
57182.583973	11.22922	0.03476	27.98556	− 0.23481
57183.570990	16.72535	0.03284	27.84478	− 0.14822
57184.619044	13.51188	0.03994	28.02373	0.01529
57199.571858	19.70855	0.04228	27.54479	− 0.61449
57202.552044	10.48449	0.03984	28.13346	− 0.40772
57203.556020	18.14702	0.04130	27.74655	− 0.40814
57204.548030	12.83536	0.03205	28.24409	− 0.43471
57486.697998	19.76909	0.03492	27.99402	− 0.27572
57487.645330	9.56572	0.03248	28.20436	− 0.32989
58198.758018	9.99469	0.03287	27.88726	0.24160
58199.708869	17.65346	0.03003	27.82458	0.08529

Note. [a]Marks data that were excluded from the fit.

Table A2. CORALIE (1) radial velocity data set. Machine readable format is available online at CDS.

BJD_{UTC}	RV ($km\,s^{-1}$)	σ ($km\,s^{-1}$)	FWHM ($km\,s^{-1}$)	BIS ($km\,s^{-1}$)
56449.553799	9.66479	0.07635	27.71726	0.39581
56684.776572	19.97341	0.08458	28.16283	− 0.18934
56687.719393	12.26985	0.08186	27.55700	− 0.23831
56690.804858	13.74564	0.08728	28.12772	0.13317
56692.786749	10.85002	0.07247	27.75353	− 0.01915
56693.785368	19.51221	0.07121	27.96600	− 0.04120
56694.751460	9.43889	0.07732	27.92017	− 0.20278
56696.650910	11.26911	0.07950	28.07056	− 0.37291
56697.709981	17.87517	0.07976	27.92011	− 0.31469
56714.747621	9.53700	0.10260	27.63444	− 0.81799
56718.738063	11.08132	0.07096	28.14193	− 0.27901
56722.748140	17.08727	0.07493	28.02565	− 0.30170
56726.607359	19.62246	0.08759	28.05893	0.27405
56739.667157	17.83755	0.06912	28.30868	− 0.37087
56740.828853	11.33148	0.08085	28.03725	0.18074
56743.729435	12.86017	0.08500	27.87329	− 0.47992
56748.718570	19.68182	0.07960	28.05396	0.58332
56773.547138	17.30455	0.09400	27.93314	− 0.50840
56809.616019	9.78716	0.08697	27.88691	− 0.28205
56810.576861	19.97365	0.09314	27.82375	0.03207
56811.626760	10.30808	0.08987	27.63040	− 0.42166
56833.553624	11.87092	0.08970	27.65532	− 0.32040
56837.523574	17.99888	0.10351	28.34447	0.25509
56878.471921	13.13879	0.10648	28.82110	− 0.02549
56879.472253	18.55910	0.11714	27.56328	0.27840
56880.475420[a]	10.58605	0.10760	29.58610	0.46275

Note. [a]Marks data that was excluded from the fit.

Table A3. CORALIE (2) radial velocity data set. Machine readable format is available online at CDS.

BJD_{UTC}	RV ($km\,s^{-1}$)	σ ($km\,s^{-1}$)	FWHM ($km\,s^{-1}$)	BIS ($km\,s^{-1}$)
56998.827826	17.47009	0.12933	27.08932	− 0.39700
57010.832418	10.57601	0.09756	28.24718	− 0.27460
57015.847897	18.50726	0.08972	28.09100	− 0.49615
57023.751810	9.79495	0.10472	28.25546	0.04621
57026.761266	17.05405	0.09548	27.88570	− 0.35298
57068.721936	16.92315	0.08204	27.84734	− 0.23294
57079.758041	16.58560	0.09324	27.88199	− 0.24752
57081.729334	13.31412	0.09905	27.79138	− 0.20482
57119.490788	16.66207	0.12742	27.87915	− 0.93028
57121.524136	13.88072	0.12961	27.91771	− 0.24793
57138.722837	9.73737	0.11964	28.15435	− 0.85951
57188.507306	19.25630	0.14644	28.72389	− 0.47192
57370.812711	10.00891	0.13534	28.44965	0.13814
57371.843190	19.65781	0.12413	28.39575	− 0.22403
57422.738422	18.95753	0.09442	28.50348	− 0.36238
57423.721681	9.50032	0.08920	27.99541	− 0.06870
57458.648308	11.57403	0.09403	28.15161	− 0.40348
57477.536707	18.74728	0.10241	28.08040	0.08369
57560.561020	9.27320	0.09932	28.36695	0.08509
57569.464267	9.35399	0.11077	28.10119	0.12780
57590.489717	19.78442	0.10282	27.71082	0.09967
57716.848800	15.01008	0.14879	27.54259	− 1.16172

APPENDIX B: PHOTOMETRIC INFORMATION

Table B1. Light-curve information for WASP-128.MF denotes an additional constant offset for the meridian flip.

Date	Instrument	Filter	t_{exp} s	N_{exp}	Baseline function
2013 May 31	TRAPPIST	Sloan z'	8	705	$p(t^2)$
2014 Feb 11	TRAPPIST	Sloan z'	11	832	$p(t^2)$ + MF
2014 Feb 20	TRAPPIST	Sloan z'	11	1014	$p(t^2)$
2014 Mar 03	TRAPPIST	Sloan z'	11	860	$p(t^2)$
2014 Mar 03	*Euler*	Gunn r'	60	215	$p(t^2)$ + MF
2014 Mar 25	*Euler*	Gunn r'	75	136	$p(t^2 + \mathrm{sky}^1)$
2014 May 26	*Euler*	Gunn r'	60	203	$p(t^2)$
2015 May 10	TRAPPIST	Sloan z'	8	969	$p(t^2)$ + MF

This paper has been typeset from a TEX/LATEX file prepared by the author.